# An Inverse Method Allowing User-specified Layouts of Magnetized Microfibers in Solidifying Composites

GEORGE S. DULIKRAVICH* AND MARCELO J. COLAÇO
*Mechanical & Aerospace Engineering Department,*
*MAIDO Institute, University of Texas at Arlington,*
*UTA Box 19018, Arlington, TX 76019, USA*

THOMAS J. MARTIN
*Turbine Discipline Engineering & Optimization Group,*
*Pratt Whitney Engine Company, 400 Main Street,*
*M/S 169-20, East Hartford, CT 06108, USA*

SEUNGSOO LEE
*3-3-2, Agency for Defense Development,*
*Youseong P.O. Box 35-3, Daejeon, Korea*

(Received October 11, 2002)
(Revised February 12, 2003)

**ABSTRACT:** [2]A new concept for controlled manufacturing of specialty composite materials has been developed. It is based on the concept of aligning magnetizable microfibers tangent to magnetic field lines of force. This paper offers a method that allows users to specify desired patterns of the magnetic lines of force that can be achieved by an appropriate positioning of magnets of various strengths along the boundaries of the composites' curing container. An improved analytical model and a numerical algorithm have been developed for the prediction of the magnetic force lines inside a flowing and solidifying melt. This analysis code was combined with a hybrid constrained optimization algorithm that minimizes a normalized sum of least square differences between the user-specified and the predicted patterns of the magnetic lines of force. This software package was used to inversely evaluate the strengths, locations, and orientations of magnets needed to generate the user-specified patterns of the magnetic lines of force in the solidifying composite thus verifying the conceptual feasibility of this novel manufacturing process.

**KEY WORDS:** magneto-hydro-dynamics, composite materials, solidification, inverse problems, optimization.

*Author to whom correspondence should be addressed. E-mail: dulikra@mae.uta.edu



0021-9983/0?/00 0001–15 $10.00/0 DOI: 10.1177/002199802034308

## INTRODUCTION

IT IS WELL known that defects in short fiber composites are often due to uncontrolled fiber orientation and concentration during composites manufacturing [1]. These defects can significantly reduce the functionality of the composite material [15]. Also, in many applications it would be highly desirable to have directional dependence of physical properties of the material, that is, to have strongly nonisotropic materials [19]. This implies that it would be of interest to perform curing of the resin in such a way that the local concentration and orientation of the fibers is fully controlled. During a controlled solidification process from a melt, it is important to understand the process of solid phase formation. The accumulated solid phase effectively reduces and deforms the cross sectional area of the passages and causes significant local variations in pressure and melt flow-field shear stresses. During the solidification process, melt flow is generated due to strong thermal buoyancy forces. This process cannot be effectively controlled in the case of strong heat transfer, except if influenced by a global body force. One such body force is the general electromagnetic Lorentz force that is created in any electrically conducting fluid when either a magnetic field or an electric field is applied.

During the curing process in composites manufacturing, we usually work with electrically conducting liquid polymers and carbon fibers, although a variety of other molten substances and fibers made of other materials are often used. The resins are electrically conducting either because of the presence of iron atoms, salts, or acids. In addition, if short carbon fibers (5–10 μ in diameter and 200 μ long) are vapor-coated with a thin layer (2–3 μ) of a ferromagnetic material like nickel [15], the fibers will respond to the externally applied electromagnetic fields by rotating and translating so that they become aligned with the magnetic lines of force [15,21]. This is especially true for short fibers [15]. Thus, if an external magnetic field is applied, the molten resin flow-field will respond and the solid/liquid front shape and its speed could be manipulated nonintrusively [3,4,7]. Experimental confirmation of the validity of the concept of aligning magnetized microfibers tangent to the magnetic field lines was performed by Hatta and Yamashita [15]. However, no attempt was made to control the pattern of these lines.

The objective of this work is to explore the feasibility of manufacturing specialty metal matrix and polymer composite materials that will have specified (desired) locally directional variation of bulk physical properties like thermal and electrical conductivity, modulus of elasticity, thermal expansion coefficient, etc. The fundamental concept is based on specifying a desired pattern of orientations and spacing of microfibers in the final composite material product. Then, the task is to determine the proper strengths, locations, and orientations of magnets that will have to be placed along the boundaries of the curing composite part so that the resulting magnetic field lines of force will coincide with the specified (desired) pattern of the microfibers' distribution. It is important to understand that the pattern of these lines depends on the solidifying resin flow-field and the spatial variation of the applied magnetic field.

Thus, the successful proof of this controlled manufacturing concept involves the development of an appropriate software package for the numerical solution of the partial differential equation system governing magneto-hydro-dynamics (MHD) involving combined fluid flow, magnetic field, and heat transfer that includes liquid–solid phase change [5]. In addition, it involves development of a constrained optimization software that is capable of automatically determining the correct strengths, locations, and orientations of a finite number of magnets that will produce the magnetic field force

pattern which coincides with the desired and specified fiber concentration and orientation pattern in the curing composite material part.

Numerous analytical and numerical formulations have been developed for simulation of solidification processes in solidifying fluid flows with and without the influence of an externally applied steady magnetic field [5,11]. An extended form of the Boussinesq approximation allowing for temperature-dependent physical properties of the fluid including latent heat of phase change was incorporated in this formulation that simultaneously predicts detailed velocity, pressure, and temperature fields for the moving fluid while capturing the forming solid phase by using a single computer code. Computational results confirmed that the magnetic field has a profound influence on the solidifying flow-field. It reduces intensity of the flow recirculation [3,4,9] and causes distorted velocity profiles with pronounced overshoots close to the solid boundaries. This change influences heat transfer through the boundaries and consequently the amount of the solid phase accrued on undercooled walls.

## A MATHEMATICAL MODEL OF MAGNETO-HYDRO-DYNAMICS (MHD) WITH SOLIDIFICATION

The modifications to the Navier-Stokes relations for the MHD fluid flow with heat transfer and phase change come from the electro-magnetic force on the fluid where all induced electric field terms have been neglected. The latent heat released or absorbed per unit mass of mushy region (where $T_{\text{liquid}} > T > T_{\text{solid}}$) is proportional to the local volumetric liquid/(liquid + solid) ratio often modeled [20] as

$$f = \frac{V_\ell}{V_\ell + V_s} = \left(\frac{T - T_{\text{solid}}}{T_{\text{liquid}} - T_{\text{solid}}}\right)^n = \tilde{\theta}^n \tag{1}$$

Here, the exponent $n$ is typically $0.2 < n < 5$, subscripts $\ell$ and $s$ designate liquid and solid phases, respectively, while $f = 1$ for $T \geq T_{\text{liquid}}$ and $f = 0$ for $T \leq T_{\text{solid}}$. Physical properties (density, viscosity, heat conductivity, heat capacity, etc.) are often significantly different in the melt as compared to the solid phase. We may assume linear variation of density as a function of the nondimensional temperature, $\theta$, in the liquid

$$\rho_\ell = \rho_r\left[1 + \left(\frac{\partial(\rho_\ell/\rho_r)}{\partial\theta}\right)_r(\theta - \theta_r)\right] = \rho_r[1 - \alpha_\ell(\theta - \theta_r)] \tag{2}$$

with a similar expression for the solid phase. The reference values are designated with the subscript "$r$". Then, the liquid–solid mixture density and modified specific heat can be defined using an enthalpy method [18] as

$$\rho_{\text{mix}} = f\rho_\ell + (1 - f)\rho_s \tag{3}$$

$$c_{\text{mix}} = fc_\ell + (1 - f)c_s + [(T - T_s)(c_\ell - c_s) + L]\frac{df}{d\theta} \tag{4}$$

so that latent heat, $L$, is released in the mushy region according to Equation (4).

The nondimensional numbers of interest in MHD are

| Reynolds hydrodynamic | Prandtl hydrodynamic | Eckert |
|---|---|---|
| $\mathrm{Re} = \dfrac{\rho_r v_r \ell_r}{\mu_{vr}}$ | $\mathrm{Pr} = \dfrac{\mu_{\mathrm{vr}} \mathrm{c_r}}{\kappa_{\mathrm{r}}}$ | $Ec = \dfrac{v_r^2}{c_r \Delta T_r}$ |
| Grashof | Prandtl magnetic | Hartmann |
| $Gr = \dfrac{\rho_r^2 \alpha_r g_r \Delta T_r \ell_r^3}{\mu_{vr}^2}$ | $\mathrm{Pm} = \dfrac{\mu_{\mathrm{vr}} \sigma_{\mathrm{r}} \mu_{\mathrm{r}}}{\rho_{\mathrm{r}}}$ | $\mathrm{Ht} = \ell_{\mathrm{r}} \mu_{\mathrm{r}} \mathrm{H_r} \left( \dfrac{\sigma_{\mathrm{r}}}{\mu_{vr}} \right)^{1/2}$ |

where $\mu_{vr}, c_r, \kappa_r, \mu_r, L_r, \ell_r, H_r, \sigma_r, \alpha_r$ are the reference values of viscosity, specific heat, heat conductivity, magnetic permeability, latent heat of liquid–solid phase change, length, magnetic field, electric conductivity, and thermal expansion, respectively. Then, the nondimensional Navier-Stokes equations for phase-changing MHD mixtures of two liquids (solid phase is treated as the second liquid with extremely high viscosity), can be formulated [5,6,17] so that the mixture mass conservation is

$$\nabla \cdot \mathbf{v} = 0 \tag{5}$$

where $\mathbf{v}$ is the fluid velocity. The classical modeling of MHD assumes that there are no free electric charges in the fluid, there is no externally applied electric field, and that magnetic field is not time-varying [6,17]. Linear momentum conservation for two-phase incompressible MHD flows with thermal buoyancy force and magnetic force can be expressed as

$$\begin{aligned} & f\rho_\ell \nabla \cdot (\mathbf{vv} + \hat{p}_\ell \mathbf{I}) + (1-f)\rho_s \nabla \cdot (\mathbf{vv} + \hat{p}_s \mathbf{I}) \\ & \quad = f \left\{ \nabla \cdot \left[ \frac{\mu_{v\ell}}{\mathrm{Re}} (\nabla \mathbf{v} + \nabla \mathbf{v}^T) \right] + \frac{Gr}{\mathrm{Re}^2} \rho_\ell \alpha_\ell \theta \underline{g} + \frac{Ht^2}{Pm \mathrm{Re}^2} \mu_\ell (\nabla \times \mathbf{H}) \times \mathbf{H} \right\} \\ & \quad + (1-f) \left\{ \nabla \cdot \left[ \frac{\mu_{vs}}{\mathrm{Re}} (\nabla \mathbf{v} + \nabla \mathbf{v}^T) \right] + \frac{Gr}{\mathrm{Re}^2} \rho_s \alpha_s \theta g + \frac{Ht^2}{Pm \mathrm{Re}^2} \mu_s (\nabla \times \mathbf{H}) \times \mathbf{H} \right\} \end{aligned} \tag{6}$$

Here, $\mathbf{I}$ is the identity tensor. The nondimensional hydrodynamic, hydrostatic, and magnetic pressures were combined to give

$$\hat{p}_\ell = \frac{p}{\rho_\ell} + \frac{\varphi}{Fr^2} + \frac{Ht^2}{Pm \mathrm{Re}^2} \mu_\ell \mathbf{H} \cdot \mathbf{H} \quad \text{and} \quad \hat{p}_s = \frac{p}{\rho_{\mathrm{s}}} + \frac{\varphi}{Fr^2} + \frac{Ht^2}{Pm \mathrm{Re}^2} \mu_{\mathrm{s}} \mathbf{H} \cdot \mathbf{H} \tag{7}$$

where $\varphi$ is the nondimensional gravity potential defined as $\mathbf{g} = -\nabla\varphi$ and $\mathbf{H}$ is the magnetic field intensity ($\mathbf{H} = \mathbf{B}/\mu$). Then, the energy conservation for steady incompressible phase-changing MHD flows including Joule heating can be written in its nondimensional form as [5]

$$\begin{aligned} \rho_{\mathrm{mix}} \nabla \cdot (c_{\mathrm{mix}} \theta \mathbf{v}) = & f \left[ \frac{1}{R_e P_r} \nabla \cdot (\kappa_\ell \nabla \theta) + \frac{1}{\sigma_\ell} \frac{H_t^2 E_c}{P_m^2 R_e^3} (\nabla \times \mathbf{H}) \cdot (\nabla \times \mathbf{H}) \right] \\ & + (1-f) \left[ \frac{1}{R_e P_r} \nabla \cdot (\kappa_{\mathrm{s}} \nabla \theta) + \frac{1}{\sigma_{\mathrm{s}}} \frac{H_t^2 E_c}{P_m^2 R_e^3} (\nabla \times \mathbf{H}) \cdot (\nabla \times \mathbf{H}) \right] \end{aligned} \tag{8}$$

With MHD assumptions, Maxwell's system for steady electromagnetics of a moving medium becomes

$$\nabla \cdot \mathbf{B} = 0 \tag{9}$$

$$\nabla \times \mathbf{H} = \mathrm{J} \tag{10}$$

$$\nabla \cdot \mathbf{J} = 0 \tag{11}$$

Here, **J** is the electric current density. Under the MHD conditions and assuming that the fluid speed is negligible compared to the speed of light [17], Ohm's law reduces to

$$\mathbf{J} = \sigma \mathbf{v} \times \mathbf{B} \tag{12}$$

If electric conductivity and magnetic permeability are assumed constant, then the following nondimensionalized magnetic field transport equation for the phase-changing incompressible MHD flow can be obtained from Equations (9)–(12).

$$-\nabla \times (\mathbf{v} \times \mathbf{H}) = \frac{\mathrm{F}/(\sigma_\ell \mu_\ell) + (1-f)/(\sigma_s \mu_s)}{Pm\mathrm{Re}} \nabla^2 \mathbf{H} \tag{13}$$

It needs to be solved intermittently [5] with the Equations (5)–(8). The modified magnetic transport equations (13), the continuity equation (5), the modified Navier-Stokes equations (6), and the modified energy equation (8) were integrated numerically using a finite volume method for structured grids written in terms of nonorthogonal boundary-conforming coordinates [7]. Artificial density formulation was used to de-singularize the Navier-Stokes system and the artificial time integration was performed using a four-stage Runge-Kutta algorithm.

## INVERSE PROBLEM OF DETERMINING UNKNOWN MAGNETIC FIELD BOUNDARY CONDITIONS

Given a prescribed pattern of magnetic field lines, let us try to estimate the magnetic field boundary conditions that will generate such a pattern. This is a typical inverse boundary condition determination problem [12].

As the basic test geometry we considered a square container (Figure 1) filled with a molten electrically conducting silicon resin that contains a dispersed phase consisting of magnetizable microfibers. Top and bottom walls of the container were treated as adiabatic, while left vertical wall was treated as a "cold" surface with constant temperature $T_c = 1676.0\,\mathrm{K}$ that is below the solidification temperature for molten silicon. The right vertical wall was treated as a "hot" surface with temperature $T_h = 1686.0\,\mathrm{K}$ that is above the melting temperature of the silicon. Magnets of various strengths were assumed positioned orthogonal to all four boundaries of the container.

Because of the highly coupled system of nonlinear partial differential equations governing the MHD solidification, the easiest approach to solving this inverse problem is to formulate it as a least squares problem and then use an optimization algorithm to minimize the $L^2$ norm. For example, the objective function for this problem could be the

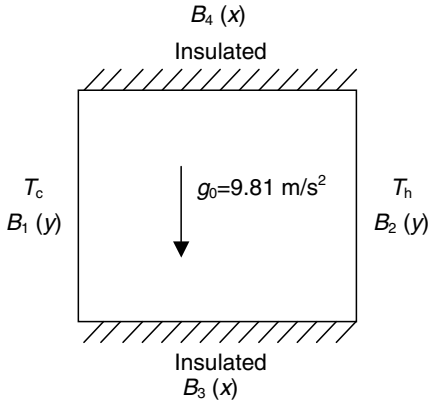


***Figure 1.*** *Geometry and boundary conditions for test cases 1 and 2.*

sum of all squared differences between the estimated and prescribed magnetic field components. The task is then to find the minimum of $F$, where $F$ is defined as

$$F = \left[ \frac{1}{\#\text{cells}} \sum_{i=1}^{\#\text{cells}} (B_x^{\text{specified}} - B_x^{\text{calculated}})^2 + \frac{1}{\#\text{cells}} \sum_{i=1}^{\#\text{cells}} (B_y^{\text{specified}} - B_y^{\text{calculated}})^2 \right]^{1/2} \tag{14}$$

since magnetization was neglected in this work. The values of the magnetic field strength throughout the domain depend strongly on the values of the magnetic field along the boundaries of the domain. Thus, the desired pattern of the magnetic field lines could be created by the yet unknown boundary values of the magnetic field. The boundary values of the magnetic field were parameterized with the following expression

$$B(x_k) = \sum_{i=1}^{M} P_i C_i(x_k) \tag{15}$$

where the $P_i$s are unknown parameters that will be found with the help of the hybrid optimization algorithm. The functions $C_i(x_k)$ are given as

$$C_i(x_k) = \cos\left[(i-1)\frac{\pi}{2}x_k\right] \quad \text{for } i = 1, 3, 5, \ldots \tag{16}$$

$$C_i(x_k) = \cos\left[i\frac{\pi}{2}x_k\right] \quad \text{for } i = 2, 4, 6, \ldots \tag{17}$$

A variety of optimization algorithms have been developed and widely used in multiple disciplines. Various optimization algorithms have been known to provide faster convergence over others depending upon the size and shape of the mathematical design space, the nature of the constraints, and where they are during the optimization process. This is why we created a hybrid constrained optimization software [13] which incorporates several of the most popular optimization modules; the Davidon-Fletcher-Powell (DFP) gradient search method, a genetic algorithm (GA), the Nelder-Mead (NM) simplex method, quasi-Newton algorithm of Pshenichny-Danilin (LM), differential evolution (DE), and sequential quadratic programming (SQP). Each algorithm provides a unique approach to optimization with varying degrees of convergence, reliability, and robustness at

different stages during the iterative optimization process. A set of analytic rules and heuristics were coded into the program to automatically switch back and forth among the different optimization algorithms as the process proceeded. Different versions of this hybrid optimization package have been successfully applied during the optimization of various multidisciplinary problems [10].

## NUMERICAL RESULTS

Three test cases were considered corresponding to three different prescribed magnetic field boundary conditions. In all test cases the initial guess for the parameters was zero, that is, the initial guess for the magnetic field was that it is zero. The hybrid optimizer started with the Differential Evolutionary method in all test cases and the initial population was randomly generated around the initial guess. The number of population members was equal to three times the number of parameters. Input parameters used in all three test cases are given in Table 1.

In test Case 1, Equation (15) was used to generate prescribed magnetic boundary conditions, where the values of the parameters $P_i$ were

$$P_1 = 0.0032; P_2 = 0.0563; P_3 = 0.2365; P_4 = 0.3658; P_5 = 0.0698; P_6 = 0.0023$$

In the inverse problem of determining the unknown magnetic field boundary conditions in test Case 1 we used three parameters for $B_1(y)$ and three parameters for $B_3(x)$, while magnetic boundary conditions on the opposite walls were enforced as periodic, that is $B_2(1, y) = B_1(0, y)$ and $B_4(x, 1) = B_3(x, 0)$.

Figure 2 shows the prescribed and the estimated boundary conditions for test Case 1. One can see that the boundary conditions for $x = 0.0$ and $x = 1.0$ are better estimated than the

***Table 1. Input values.***

| | |
|---|---|
| $\boldsymbol{l} = 0.01$ m | $\mathrm{Fr} = 8.7870 \times 10^{-2}$ |
| $\boldsymbol{B}_0 = 0.1$ T | $\mathrm{Ec} = 7.1524 \times 10^{-8}$ |
| $\mathrm{Re} = 1000$ | $\mathrm{Ht} = 4.1864 \times 10^{1}$ |
| $\mathrm{Pr} = 1.1613 \times 10^{-2}$ | $\mathrm{Gr} = 1.8132 \times 10^{5}$ |
| $\boldsymbol{V}_0 = 2.7522 \times 10^{-2}$ m/s | $\mathrm{Pm} = 1.0 \times 10^{-2}$ |

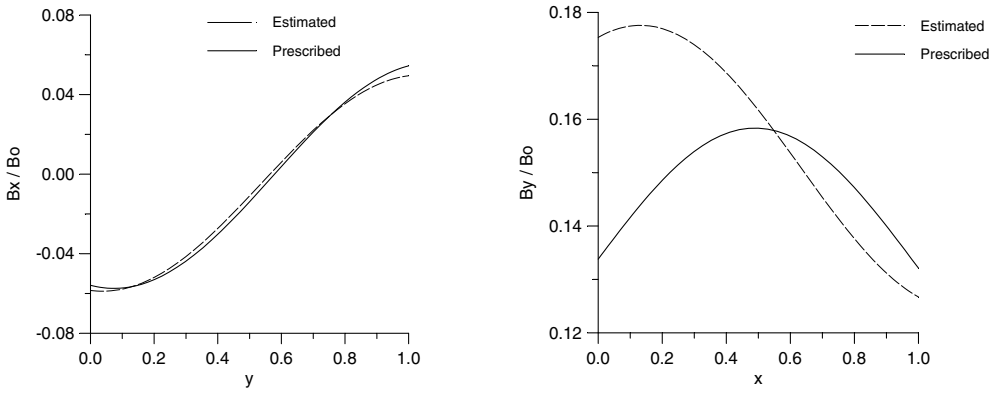


***Figure 2.*** *Specified and estimated boundary conditions for magnetic field in test case 1.*

boundary conditions for $y = 0.0$ and $y = 1.0$. Figure 3 shows the magnetic and temperature fields obtained with the prescribed boundary conditions (Figure 2) for test Case 1.

Figure 4 shows the magnetic and temperature fields for test Case 1 that were obtained from minimization of the objective function F (Equation (14)) with the use of a hybrid optimizer that varied the parameters of the boundary conditions of the magnetic field (Equation (15)). One can see that the magnetic and thermal fields obtained from this inverse methodology match the prescribed magnetic and thermal field patterns shown in Figure 3 very closely. Since all values are nondimensionalized, the value of 0.0 in the thermal field plot designates the liquid–solid interface. Finally, Figure 5 shows the convergence history of the optimization process. In this case, the major optimization modules applied were the GA and the SQP modules.

Figure 6 shows the prescribed and the estimated magnetic boundary conditions for test Case 2, where a discontinuous function was considered specified on the vertical wall. In this case, $B_1(0, y)$ was approximated with only six parameters although the actual value

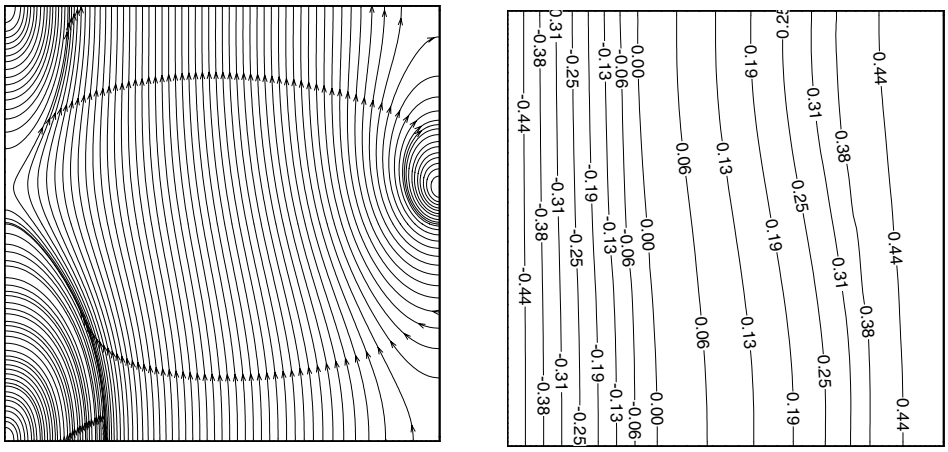


***Figure 3.*** *Specified magnetic and temperature field distributions for test case 1.*

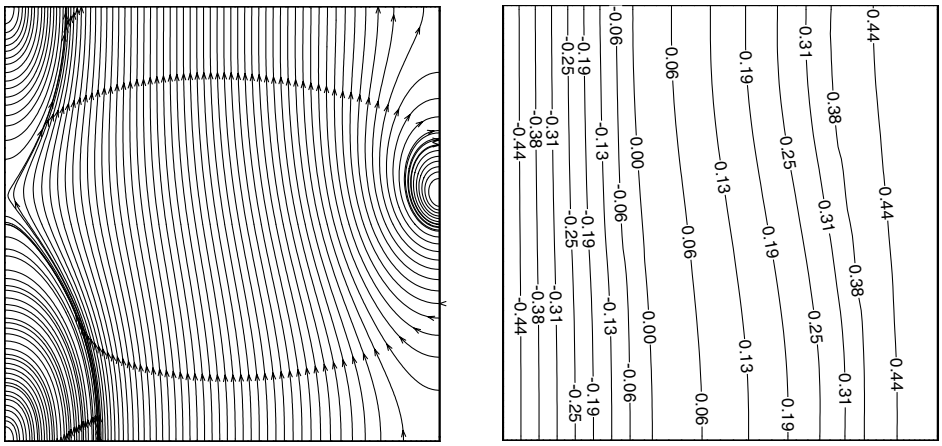


***Figure 4.*** *Calculated magnetic and temperature field distributions for test case 1.*

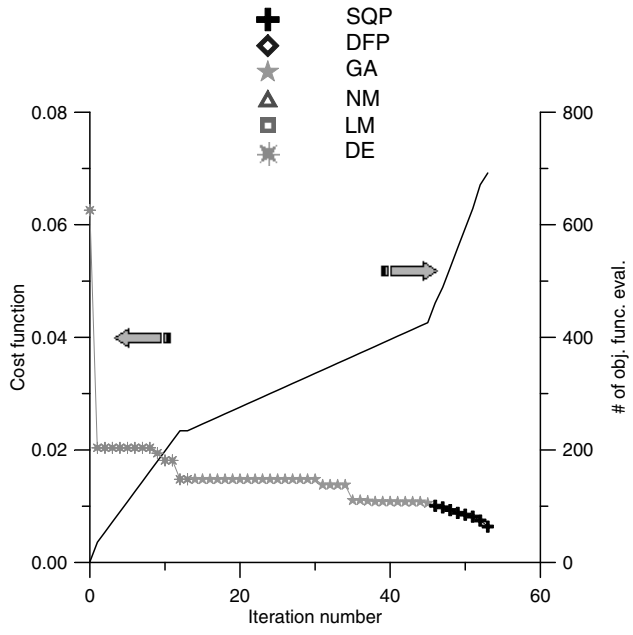


***Figure 5.*** *Convergence history for the hybrid optimization for test case 1.*

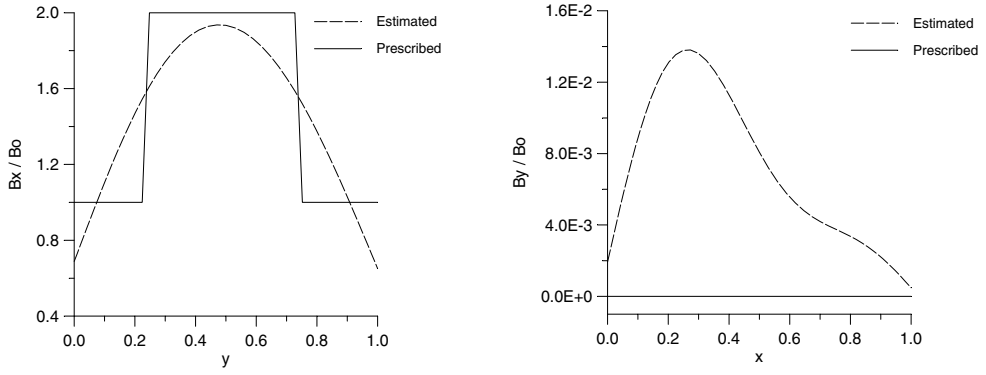


***Figure 6.*** *Specified and estimated boundary conditions for magnetic field in test case 2.*

was a discontinuous function. The value of $B_3(x, 0)$ was similarly approximated with six parameters although the actual value was a constant. Magnetic boundary conditions on the opposite walls were enforced as periodic, that is $B_2(1, y) = B_1(0, y)$ and $B_4(x, 1) = B_3(x, 0)$. Again, the boundary conditions for $x = 0.0$ and $x = 1.0$ were better estimated than the boundary conditions for $y = 0.0$ and $y = 1.0$. The discontinuous character of the actual magnetic boundary condition for $x = 0.0$ and $x = 1.0$ could have been better estimated if more parameters were used for the trial functions given by Equation (15). Figure 7 shows the magnetic and temperature field distributions obtained with the specified boundary conditions (Figure 6) for test Case 2.

Figure 8 shows the estimated magnetic and temperature fields distribution for test Case 2. One can see that they have the same shape of the prescribed fields depicted in Figure 7, except for the magnetic lines close to the boundaries $y = 0.0$ and $y = 1.0$. Figure 9 shows

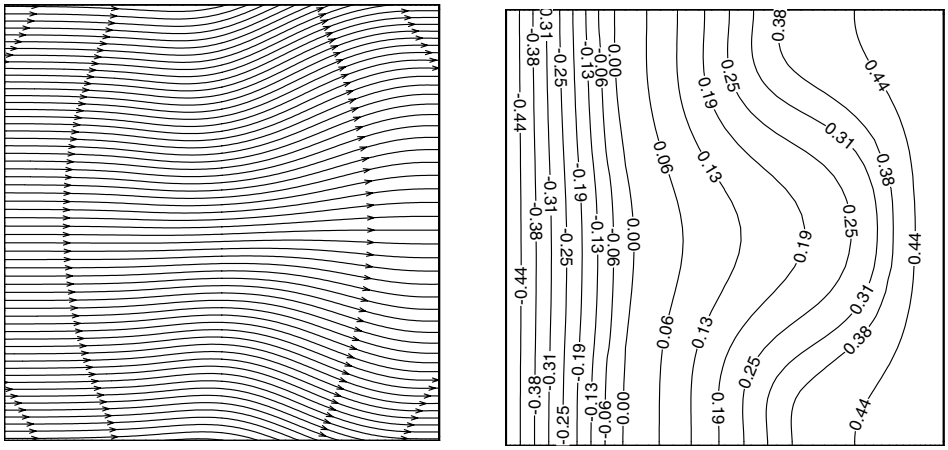

***Figure 7.*** *Specified magnetic and temperature field distributions for test case 2.*

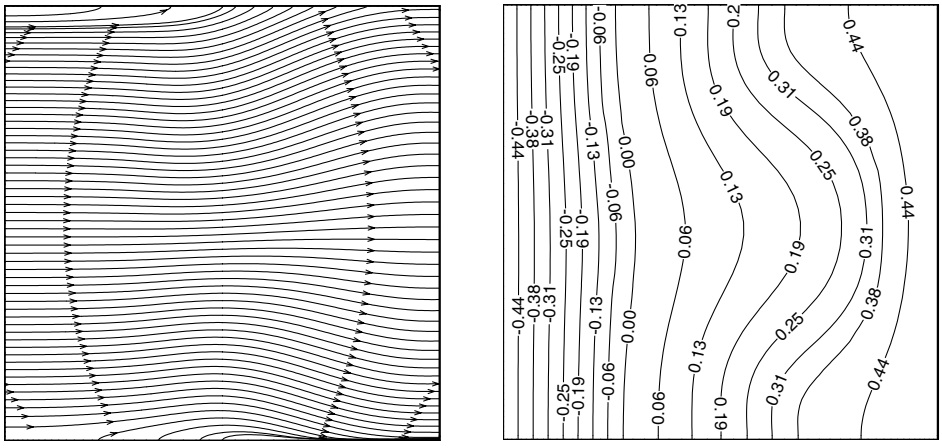

***Figure 8.*** *Calculated magnetic and temperature field distributions for test case 2.*

the convergence history, where one can see that the DE optimization module did not have a satisfactory performance in this case. In fact, for this case, the major optimization module was the GA.

It should be pointed out that these test cases used physical properties for silicon. The exception was the magnetic Prandtl number for which a value, which is three orders of magnitude larger than the physical value, was used. This was done because the realistic extremely small values of $P_m$ were causing the explicit numerical integration algorithm used in the MHD analysis to diverge. In addition, the value of viscosity coefficient in the solid phase was treated as only two orders of magnitude higher than in the liquid. Higher values of this artificial viscosity were causing the MHD analysis code to oscillate. As a result of using the lower values of the viscosity in the locally solidified locations, the local velocities predicted in the solid phase were not negligible. They needed to be explicitly reinitialized to zero values after each iterative sweep through the computational domain. This slowed the convergence rate of the MHD analysis significantly.

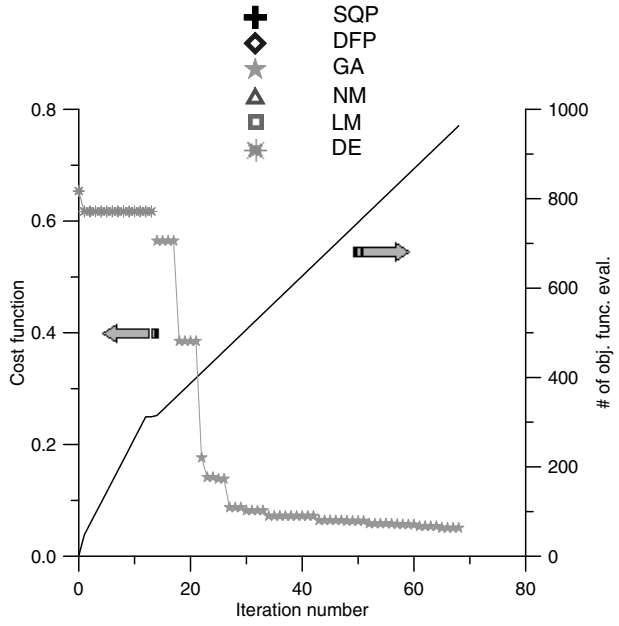


***Figure 9.*** *Convergence history for the hybrid optimization for test case 2.*

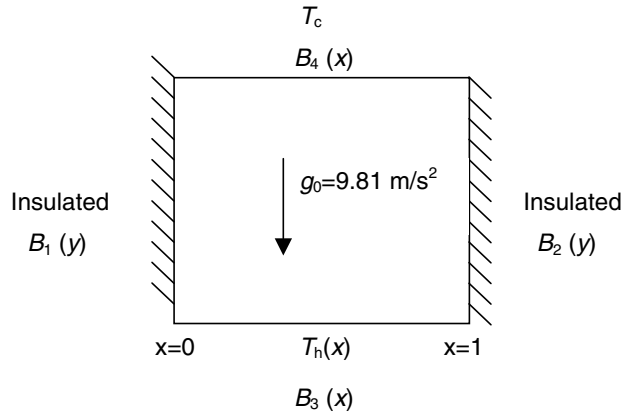


***Figure 10.*** *Normalized geometry and thermal boundary conditions for test case 3.*

For the Case 3, the following problem was considered, using the same parameters of Table 1. Vertical walls were adiabatic (Figure 10), top wall was at $T_c = 1676.0\,\mathrm{K}$ and bottom wall was at $T_h(x) = 4(-x^2 + x) + 1686.0\,\mathrm{K}$. In this case, three separate parameters were used to parameterize each of the four magnetic boundary conditions, where $B_1(0, y) \neq B_2(1, y)$ and $B_3(x, 0) \neq B_4(x, 1)$. That is, magnetic field boundary conditions were not explicitly treated as periodic. Figure 11 shows the prescribed and the estimated magnetic boundary conditions for test Case 3. Figure 12 shows the prescribed magnetic and temperature field patterns obtained with the magnetic field boundary conditions as specified in Figure 11. Figure 13 shows the estimated patterns of these fields obtained by

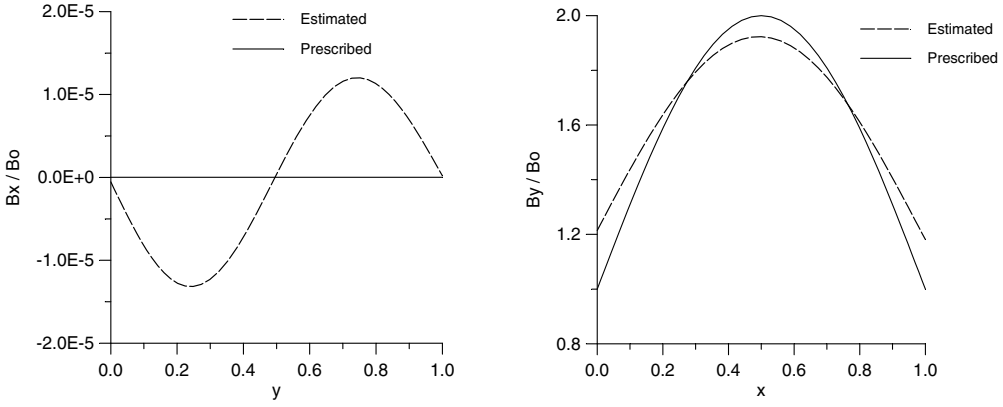


***Figure 11.*** *Specified and estimated boundary conditions for magnetic field in test case 3.*

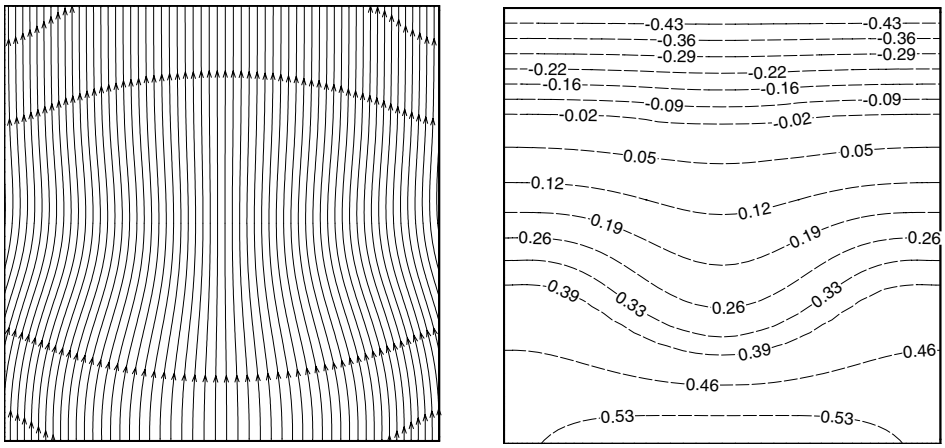


***Figure 12.*** *Specified magnetic and temperature field distributions for test case 3.*

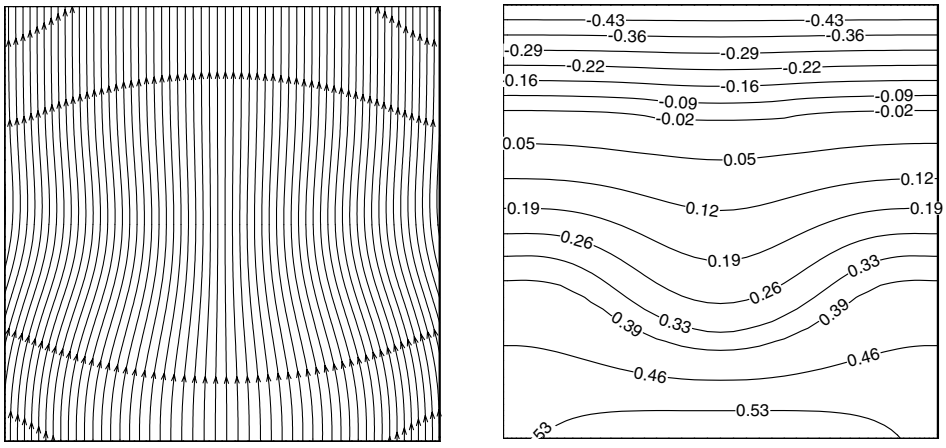


***Figure 13.*** *Calculated magnetic and temperature field distributions for test case 3.*

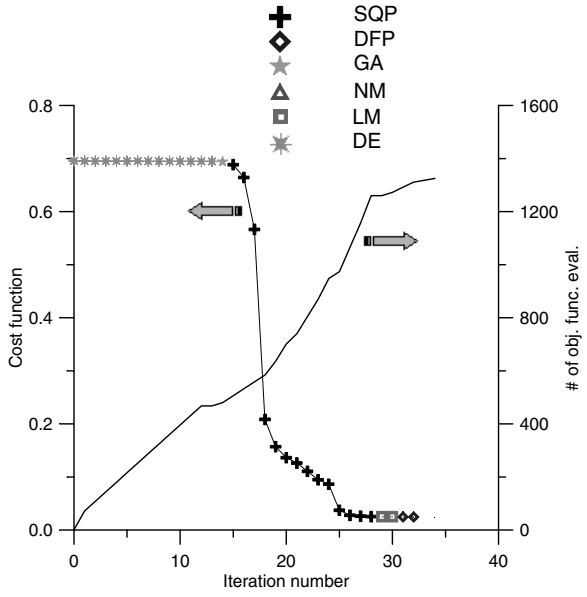


***Figure 14.*** *Convergence history for the hybrid optimization for test case 3.*

optimizing $3 \times 4 = 12$ parameters describing the boundary values of the magnetic field. The specified and the optimized patterns of the magnetic and temperature fields match each other well.

Finally, Figure 14 shows that the SQP optimization module performed the entire task in Case 3.

## DISCUSSION

In this proof-of-the-concept effort the objective was not to develop the most advanced MHD analysis involving solidification. The objective was to demonstrate the feasibility of the entire concept of inversely determining the unknown boundary values of the magnetic field that will create a user-specified pattern of the magnetic lines of force. In this study, a number of assumptions were made concerning physics of the problem. For example, all physical properties were treated as constants instead of as functions of temperature. Transport equation for the passive scalar (concentration of the microfibers) was not included, but could be added relatively easily [16]. Its addition would enable us to predict and possibly control the distribution of the microfibers along the magnetic field lines of force. Thermal stresses in the accrued solid were not analyzed since such solids are by definition nonisotropic. Different options for treating the mushy region were not exercised [18]. Other, possibly more robust and accurate numerical integration methods were not explored [4,14] that could allow for physical values of the magnetic Prandtl number and for significantly higher values of viscosity used in the solid region. Magnetization effects and fiber–resin interface drag were neglected. Also, possible effects of the material properties and the thickness and shape of the container walls were not included via a conjugate analysis [2]. Finally, the current effort neglects the fact that the entire problem of having magnetizable microfibers orient themselves tangent to the

prescribed magnetic field pattern is feasible only if the prescribed pattern is enforced in the moving and deforming mushy region. This mandates that the entire problem should in reality be treated as an unsteady control problem where boundary values of the magnetic field should vary in time. All of these details could and should be incorporated in the future work and compared to actual experimental results since this concept could be extended to manufacturing of three-dimensional composite objects and functionally graded objects of arbitrary shape.

## SUMMARY

Feasibility of a new concept has been demonstrated for manufacturing composite materials where microfibers will align along a user-specified desired pattern of the magnetic lines of force. This was accomplished by combining an MHD analysis code capable of simultaneously capturing features of the melt flow-field and the accrued solid, and a hybrid constrained optimization code. The computed pattern of the magnetic lines of force was shown to closely replicate the specified pattern when the optimizer minimized the $L^2$-norm of the difference between these two patterns. This minimization process was achieved by optimizing a finite number of parameters describing analytically the distribution and the orientations of the boundary values of the magnetic field.

## ACKNOWLEDGMENTS

The second author is grateful for the postdoctoral fellowship received from University of Texas at Arlington and from CNPq, a Brazilian council for scientific and technological development.

## REFERENCES

1. Cranston, J.J. and Reitz, J.A.III. (1980). SMC Molding Techniques for Optimized Mechanical Properties in Structural Applications, *Polymer and Plastics Technology and Engineering*, **15**: 97–3114.
2. Dennis, B.H. and Dulikravich, G.S. (2000). Simulation of Magnetohydrodynamics with Conjugate Heat Transfer, In: Onate, E., Bugeda, G. and Suarez, B. (eds), *European Congress on Computational Methods in Applied Sciences and Engineering – ECCOMAS2000*, Barcelona, Spain, 11–14 September.
3. Dennis, B.H. and Dulikravich, G.S. (2001). Optimization of Magneto-Hydrodynamic Control of Diffuser Flows Using Micro-Genetic Algorithm and Least Squares Finite Elements, *J. Finite Elements in Analysis and Design*, **37**(5): 349–363.
4. Dennis, B.H. and Dulikravich, G.S. (2002). Magnetic Field Suppression of Melt Flow in Crystal Growth, *International J. Heat and Fluid Flow*, **23**(3): 269–277.
5. Dulikravich, G.S. (1999). Electro-Magneto-Hydrodynamics and Solidification, Chapter No. 9, In: Siginer, D.A., De Kee, D. and Chhabra, R.P. (eds), *Advances in Flow and Rheology of Non-Newtonian Fluids*, *Part B*, Rheology Series, 8, pp. 677–716, Elsevier Publishers.
6. Dulikravich, G.S. and Lynn, S.R. (1995). Unified Electro-Magneto-Fluid Dynamics (EMFD): A Survey of Mathematical Models, *International J. Non-Linear Mechanics*, **32**(5): 923–932.
7. Dulikravich, G.S., Ahuja, V. and Lee, S. (1993). Three-Dimensional Control of Crystal Growth Using Magnetic Fields, SPIE paper 1916–07, In: *Proceedings of Smart Structures and Materials Conf.*, Albuquerque, New Mexico, 1–4 February.

8. Dulikravich, G.S., Ahuja, V. and Lee, S. (1994). Modeling Three-Dimensional Solidification with Magnetic Fields and Reduced Gravity, *International J. Heat and Mass Transfer*, **37**(5): 837–853.
9. Dulikravich, G.S., Choi, K.-Y. and Lee, S. (1994). Magnetic Field Control of Vorticity in Steady Incompressible Laminar Flows, ASME WAM'94, Siginer, D.A., Kim, J.H., Sheriff, S.A. and Colleman, H.W. (eds), Chicago, IL, Nov. 6–11, 1994, ASME FED-Vol. 205/AMD-Vol. 190, pp. 125–142.
10. Dulikravich, G.S., Dennis, B.H., Martin, T.J. and Egorov, I.N. (2002). In: Giannakoglou, K., Tsahalis, D.T., Periaux, J. and Fogarty, T. (eds), *Multi-disciplinary Design Optimization*, in *EUROGEN 2001 – Evolutionary Methods for Design, Optimization and Control with Applications to Industrial Problems*, Athens, Greece, Sept. 19–21, 2001, Published by International Center for Numerical Methods in Eng. (CIMNE), pp. 11–18, Barcelona, Spain.
11. Dulikravich, G.S., Kosovic, B. and Lee, S. (1993). Magnetized Fiber Orientation Control in Solidifying Composites: Numerical Simulation, *ASME J. Heat Transfer*, **115**: 255–262.
12. Dulikravich, G.S., Martin, T.J. and Dennis, B.H. (1999). Multidisciplinary Inverse Problems, In: Woodbury, K. (ed.), 3rd International Conference on Inverse Problems in Engineering (3icipe): Theory and Practice, Port Ludlow-Puget Sound, WA, June 13–18, 1999, pp. 1–8, ASME Engineering Foundation Publications.
13. Dulikravich, G.S., Martin, T.J., Dennis, B.H. and Foster, N.F. (1999). Multidisciplinary Hybrid Constrained GA Optimization, Chapter 12 In: Miettinen, K., Makela, M.M., Neittaanmaki, P. and Periaux, J. (eds), *EUROGEN'99 – Evolutionary Algorithms in Engineering and Computer Science: Recent Advances and Industrial Applications*, pp. 233–259, John Wiley & Sons, Jyvaskyla, Finland.
14. Fedoseyev, K.I., Kansa, E.J., Marin, C. and Ostrogorsky, A.G. (2001). Magnetic Field Suppression of Semiconductor Melt Flow in Crystal Growth: Comparison of Three Methods for Numerical Modeling, *Japanese CFD Journal*, **9**: 325–333.
15. Hatta, H. and Yamashita, S. (1988). Fiber Orientation Control by Means of Magnetic Moment, *J. Composite Materials*, **22**: 484–500.
16. Hirtz, J.M. and Ma, N. (2000). Dopant Transport During Semiconductor Crystal Growth: Axial versus Transverse Magnetic Field, *J. Crystal Growth*, **210**: 554–572.
17. Ko, H.-J. and Dulikravich, G.S. (2000). A Fully Non-Linear Model of Electro-Magneto-Hydrodynamics, *International J. Non-Linear Mechanics*, **35**(4): 709–719.
18. Poirier, D. and Salcudean, M. (1986). On Numerical Methods Used in Mathematical Modeling of Phase Change in Liquid Metals, ASME paper 86-WAM/HT-22, Anaheim, California, 7–12 December.
19. Smith, M.E., Benicewicz, B.C., Douglas, E.P., Earls, J.D. and Priester, R.D. Jr. (1996). Effect of High Magnetic Fields on Orientation and Properties of Liquid Crystalline Thermosets, *Polym. Prepr. Am. Chem. Soc., Div. Polym. Chem.*, **37**(1): 50–1.
20. Voller, V.R. and Swaminathan, C.R. (1991). General Source-Based Method for Solidification Phase Change, *Numerical Heat Transfer, Part B*, **19**: 175–189.
21. Yamashita, S., Hatta, H., Sugano, T. and Murayama, K. (1989). Fiber Orientation Control of Short Fiber Composites: Experiment, *J. Composite Materials*, **23**: 32–41.